Cell Host & Microbe
Article

Structural Basis for Activation and Inhibition of the Secreted *Chlamydia* Protease CPAF

Zhiwei Huang,[1,2] Yingcai Feng,[2] Ding Chen,[3] Xiaojing Wu,[2] Siyang Huang,[2] Xiaojun Wang,[2] Xingguo Xiao,[1] Wenhui Li,[2] Niu Huang,[2] Lichuan Gu,[4] Guangming Zhong,[3] and Jijie Chai[2,*]
[1]College of Biological Sciences, China Agricultural University, Beijing 100094, China
[2]National Institute of Biological Sciences, Beijing 102206, China
[3]Department of Microbiology and Immunology, University of Texas Health Science Center, San Antonio, TX 78229, USA
[4]State Key Lab of Microbial Technology, Shandong University, Shandong 250100, China
*Correspondence: chaijijie@nibs.ac.cn
DOI 10.1016/j.chom.2008.10.005

SUMMARY

The obligate intracellular pathogen *Chlamydia trachomatis* is the most common cause of sexually transmitted bacterial disease. It secretes a protease known as chlamydial protease/proteasome-like activity factor (CPAF) that degrades many host molecules and plays a major role in *Chlamydia* pathogenesis. Here, we show that mature CPAF is a homodimer of the catalytic domains, each of which comprises two distinct subunits. Dormancy of the CPAF zymogen is maintained by an internal inhibitory segment that binds the CPAF active site and blocks its homodimerization. CPAF activation is initiated by *trans*-autocatalytic cleavage, which induces homodimerization and conformational changes that assemble the catalytic triad. This assembly leads to two autocatalytic cleavages and removal of the inhibitory segment, enabling full CPAF activity. CPAF is covalently bound and inhibited by the proteasome inhibitor lactacystin. These results reveal the activation mechanism of the CPAF serine protease and suggest new opportunities for anti-*Chlamydia* drug development.

INTRODUCTION

Chlamydiae represent a group of obligate intracellular bacterial pathogens, consisting of multiple species infecting a wide range of animal hosts. Of medical importance are the species *Chlamydia trachomatis* and *Chlamydia pneumoniae*. *C. trachomatis* infect humans in both the ocular epithelia, causing preventable blindness, and urogenital tract epithelia, being a leading cause of sexually transmitted bacterial diseases with 90 million new cases each year worldwide (Brunham and Rey-Ladino, 2005). Women infected with *C. trachomatis* in the urogenital tract can develop pelvic inflammatory diseases, ectopic pregnancy, and infertility. The *C. pneumoniae* are common respiratory pathogens in humans (Brunham and Rey-Ladino, 2005), and respiratory infection with *C. pneumoniae* is associated with cardiovascular diseases and pathologies in other systems (Belland et al., 2004; Campbell and Kuo, 2004; Danesh et al., 1997).

Despite the severe health problems posed by chlamydial infection, the pathogenic mechanisms are still not well understood. It is believed that Chlamydia-induced diseases largely result from inflammatory responses provoked during chlamydial infection (Morrison et al., 1989; Rasmussen et al., 1997; Stephens, 2003). To survive in the infected hosts, Chlamydia has evolved diverse strategies to escape host immune responses (Dean and Powers, 2001; Fan et al., 1998; Greene et al., 2004; Perfettini et al., 2002; Zhong et al., 1999, 2000, and 2001). Chlamydia can evade both immune recognition and immune effector mechanisms by suppressing major histocompatibility complex (MHC) antigen expression and blocking apoptosis in the infected cells (Byrne and Ojcius, 2004; Fan et al., 1998; Fischer et al., 2004; Greene et al., 2004; Miyairi and Byrne, 2006). A Chlamydia-secreted protease designated as chlamydial protease/proteasome-like activity factor (CPAF) contributes to Chlamydia for evading host defenses by degrading host transcription factors, the regulatory factor X 5 (RFX5), and upstream stimulation factor 1 (USF-1) that are required for MHC antigen expression (Zhong et al., 2001). Degradation of the proapoptotic BH3-only proteins by CPAF (Pirbhai et al., 2006; Paschen et al., 2008) can play a role in blocking apoptosis in the infected cells. In addition, CPAF can also cleave cytokeratin 8, which may aid in chlamydial inclusion expansion (Dong et al., 2004a).

CPAF is a conserved molecule among chlamydial species and synthesized as a catalytically inactive zymogen with a molecular weight of ~70 kDa. However, the active CPAF is composed of a 29 kDa N-terminal (CPAFn) and a 35 kDa C-terminal fragment (CPAFc) (Dong et al., 2004b) and is notably shorter than the zymogen. Cleavage of the full-length CPAF into CPAFc/n and intramolecular dimerization are both necessary and sufficient for conversion of CPAF zymogen into its active form (Dong et al., 2004c), which is likely an autocatalytic process (Paschen et al., 2008). This activation mechanism is highly conserved among CPAFs from different chlamydial species (Shaw et al., 2002; Dong et al., 2005) and biologically relevant since CPAF from the clinical isolates is also processed into CPAFc and CPAFn (Dong et al., 2004b).

Although it is clear that CPAF is capable of proteolytically targeting various different host molecules, the mechanisms underlying CPAF activation and catalysis are unknown. In this study, we carried out biochemical and structural characterizations of CPAF and found that CPAF is a serine (Ser) protease with a water-mediated catalytic triad and a fully active CPAF is

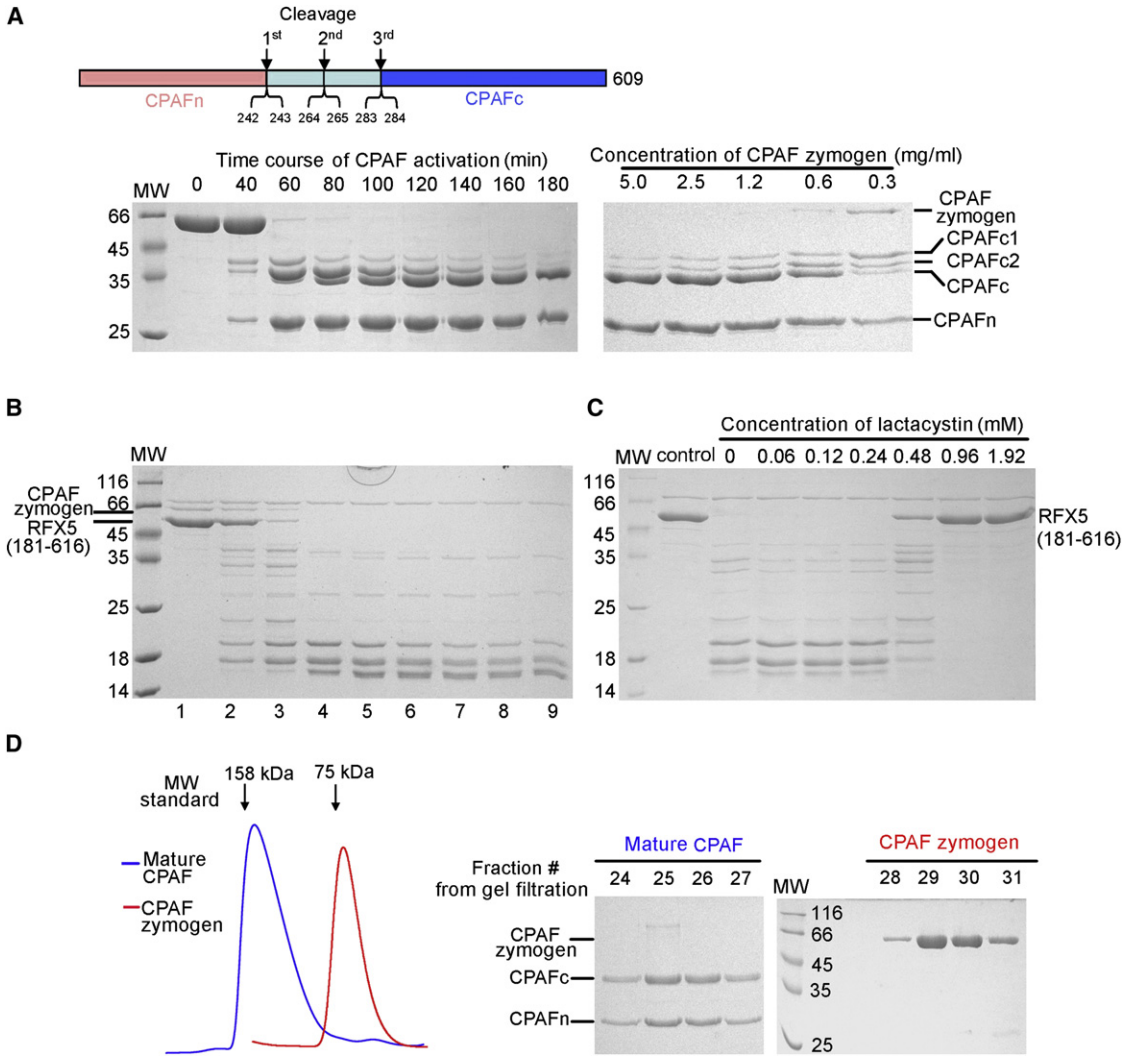

Figure 1. Autocatalytic Cleavage of CPAF Zymogen Induces Its Activation and Formation of a Stable Homodimer in Solution

All of the proteins were visualized by Coomassie blue staining following SDS-PAGE.

(A) The CPAF zymogen undergoes autocatalytic cleavages and produces the mature enzyme. (Top) CPAF was incubated at room temperature for the time as indicated, and then an equal volume of 2 × SDS buffer was added. CPAFc1, CPAFc2, and CPAFc start with residues Arg243, Val265, and Gly284, respectively. (Right) Autocatalytic cleavage of CPAF is concentration dependent. CPAF zymogen proteins with different concentration as indicated were incubated at room temperature for 3 hr before an equal volume of 2 × SDS buffer was added.

(B) The autocleaved CPAF actively degrades the CPAF substrate, RFX5. Proteins shown on the left panel of (A) were taken out at different time points and diluted 20-fold for the activity assay. The diluted CPAF was incubated with its substrate RFX5 (residues 181–616) at 4°C for 5 min.

(C) The activity of CPAF to degrade RFX5 is inhibited by the proteasome-specific inhibitor lactacystin. CPAF was incubated (for 20 min) with a different concentration of lactacystin, as indicated, before the substrate RFX5 was added.

(D) Autocleavage of CPAF induces its homodimerization. The wild-type CPAF zymogen exists primarily as a monomer, but the autocleaved CPAF exists as a homodimer in solution. Shown on the left panel is a superposition of the gel filtration chromatograms for the CPAF zymogen (red) and the purified autocleaved CPAF (blue), and the right panel shows the peak fractions. MW, molecular weight (kDa).

a homodimer (CPAFc/n:CPAFc/n). Activation of CPAF is initiated by sequential autocatalytic cleavages of an internal inhibitory segment that binds to the active site of CPAF and blocks its homodimerization. A variant of the inhibitory segment interacted with the mature CPAF and inhibited its activity in vitro. The current study has provided both the molecular basis for understanding how CPAF contributes to chlamydial pathogenesis and the essential information for developing specific inhibitors to regulate CPAF activity and potentially attenuate chlamydial pathogenicity.

RESULTS

Concentration-Dependent Autocatalytic Cleavages of CPAF Induce Its Activation

Although purified CPAF (residues 25–609) initially existed as a single-chain protein, it quickly underwent autocatalytic cleavages to generate CPAFn and CPAFc when incubated at room temperature, with two intermediates (labeled as CPAFc1 and CPAFc2) preceding the formation of CPAFc (Figure 1A, left

panel). N-terminal peptide sequencing (data not shown) indicated that the mature CPAFc starts at Gly284 as previously reported (Dong et al., 2004b), whereas CPAFc1 starts at Arg243 and CPAFc2 starts at Val265. The sequential autocatalytic cleavage of CPAF was concentration dependent (Figure 1A, right panel), suggesting that protein concentration may be critical for CPAF activation in vivo (see Discussion). In addition, environmental factors such as pH and salt concentration might also affect CPAF activation. To test whether the autocleaved CPAF is active, we compared the autocleaved CPAF with zymogen CPAF for their ability to cleave RFX5, a known cellular target of CPAF in Chlamydia-infected cells (Zhong et al., 2001). CPAF after autocleavage (lanes 2–9), but not the zymogen (lane 1), rapidly processed RFX5 into smaller fragments (Figure 1B), indicating that autocleavage of CPAF induces its activation. A similar result was also obtained when an N-terminal fragment of RFX5 was used as the substrate (Figure S1 available online). The CPAF-catalyzed cleavage of RFX5 was sensitive to the inhibition by lactacystin (Figure 1C), a proteasome inhibitor (Fenteany et al., 1995) known to inhibit CPAF activity (Zhong et al., 2001).

CPAF zymogen exhibited a molecular weight corresponding to the predicted 66 kDa under the gel filtration assay (Figure 1D). In contrast, the mature CPAF was eluted at the position of a molecular weight of about 120 kDa, although the mature CPAF is supposed to be shorter than the zymogen due to removal of about 40 amino acids during maturation. These results indicate that CPAF activation is accompanied by formation of a stable homodimer in solution.

CPAF Is a Ser Protease with Two Subunits and a Water-Mediated Catalytic Triad

To understand the catalysis mechanism of CPAF, we determined its crystal structure. Because of its higher resolution, we limit our discussions to the structure of CPAF crystallized in $P2_12_12_1$ (Table S1).

The mature CPAF consists of two structural domains, representing CPAFn and CPAFc (Figure 2A). The N terminus of CPAFn forms a three-helix bundle (α1, α3, and α4) followed by a short β strand (β1). At the other end of CPAFn is a severely twisted five-stranded β sheet (β3, β4, β5, β7, and β8). Located between the three-helix bundle and the β sheet are a short three-stranded β sheet (β2, β6, and β9) and two α helices (α5 and α6) that are almost perpendicular to each other. At one end of CPAFc is a six-stranded β sheet (β10, β11, β12, β13, β15, and β16) flanked by helices α8, α9, and α13 on one side and α15 on the other. In the middle of CPAFc are four β strands (β14, β17, β18, and β19) (Figure 2A). β18 forms an antiparallel β sheet with β1 from CPAFn, whereas β14 and the N terminus of the long loop linking α12 and β15 contact with the three α helices (α10, α11, and α12) located at the other end of CPAFc (Figure 2A).

Interaction between CPAFn and CPAFc (heterodimerization) is mediated by multiple regions of contacts. Between the two subunits is a large groove (Figure S2), which is presumably the active site of CPAF. The N-terminal three-helix bundle appears to play a prominent role in CPAF heterodimerization, because it not only interacts with β18 and its preceding loop, but also, at its one end, stacks against around the end of β14 and the start of β19 in CPAFc (Figure 2A). CPAF heterodimerization also results from package of the start of α6 against the two loops following β15 and β16. Additionally, interactions of the short α helix α14 from CPAFc with β3 and β4 from CPAFn provide further binding affinity for CPAF heterodimerization (Figure 2A).

DALI search identified D1P, a member of the C-terminal processing peptidases (CPPs) (Rawlings et al., 2008), from plant as the closest homolog of CPAF, with an rmsd of 1.75 Å over 156 Cα atoms of CPAFc (Figure 2B), mainly clustering around the primary sequence-conserved portion. This is consistent with the genomics study showing that *Chlamydiaceae* possess a high proportion of genes with highest similarity to the sequences of plant genes (Stephens et al., 1998). Ser372 and Lys397 that form the catalytic dyad in D1P (Liao et al., 2000) are well superimposed with the highly conserved (Figure S3) Ser499 and His105 in CPAF, respectively (Figure 2B). There are no other polar residues close enough to hydrogen bond with Ser499 or His105. These results suggest that CPAF is a Ser protease that utilizes Ser499 and His105 for its catalytic activity (Figure 2C). Consistently, mutations of either of these two residues completely abolished the ability of CPAF to autoprocess and cleave RFX5 (Figure 2D). Although CPAF lacks an Asp residue to form a catalytic triad as seen in a classic Ser protease (Hedstrom, 2002), a water molecule-mediated hydrogen bond between His105 and Glu558 (Figure 2C) may assist the former in activating Ser499 for the catalytic activity of CPAF. Supporting its role in the catalytic reaction, the mutant E558Q failed to autocleave and process RFX5 even after a prolonged incubation time (Figure 2D). Although DALI did not identify tricorn (Tamura et al., 1996), another member of CPPs, as a structural homolog of CPAF, three residues from its catalytic tetrad (Brandstetter et al., 2001), His746, Ser965, and Glu1023, were well superimposed with those of CPAF in the active site (Figure 2E). Moreover, the water molecule is located close to Ser745 (Figure 2E), another residue from the catalytic tetrad of tricorn, further supporting that His105, Ser499, Glu558, and the water molecule form a water-mediated catalytic triad of CPAF (Figure 2C). Our structural observations and biochemical analyses confirm that CPAF is a Ser protease, and we suggest that catalysis may be aided by a water-mediated catalytic triad.

Homodimeric Assembly of the Mature CPAF

In the crystals, each asymmetric unit contains two mature CPAF molecules, and their interaction is predominantly mediated by the packing of α1and β17 together with its preceding loop from each monomer (Figure 3A). In each monomer, Phe45, Val52, and Pro534 form extensive hydrophobic contacts with their neighboring residues from the other one (Figure 3B). Additionally, CPAF homodimerization also involves interactions of α7 and its following loop from one monomer with CPAFc from the other (Figures 3A and 3C).

To assess the functional significance of CPAF homodimerization, we made mutations for the residues at the homodimer interface and assayed the mutants for their oligomerization status and catalytic activity. One of these mutants, F45A, eluted from size exclusion column at monomer position (Figure 3D, left panel), was unable to autocleave (Figure 3D, top right) and process RFX5 (Figure 3D, bottom right). By contrast, the mutation V73D outside of the homodimer interface generated no effect on its autocleavage, homodimerization, and process of RFX5 (Figure 3D, middle panel). These results indicate that

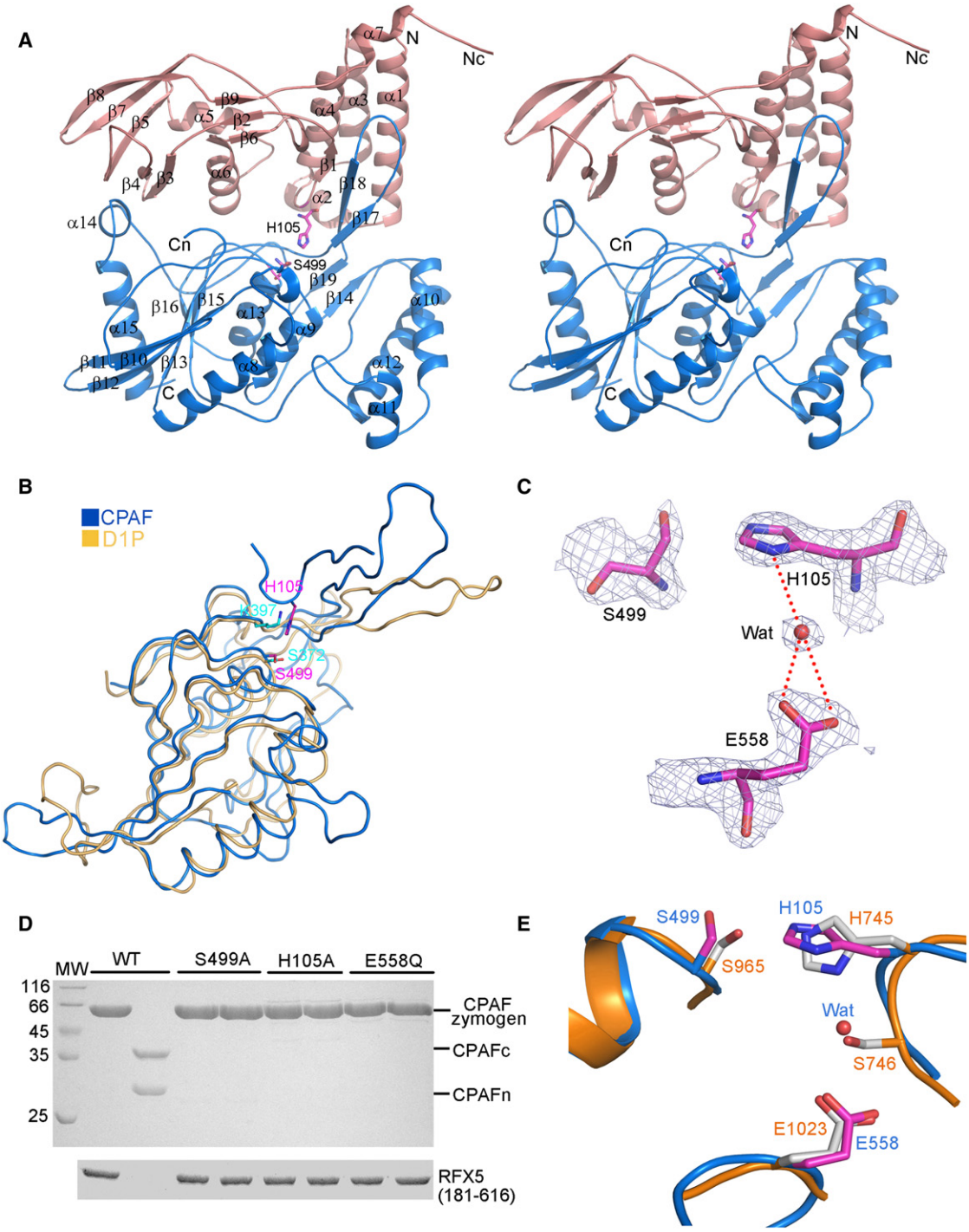

Figure 2. CPAF Is a Ser Protease with a Water-Mediated Catalytic Triad

(A) A stereo view of structure of one mature CPAF molecule. The two subunits of CPAF, CPAFn (residues 25–239), and CPAFc (residues 284–601) are colored in salmon and blue, respectively. The C terminus of CPAFn and N terminus of CPAFc are indicated by "Nc" and "Cn," respectively. The catalytic residues are shown in stick and magenta.

(B) CPAFc exhibits a similar fold to that of D1P. CPAFc and D1P are shown in blue and light orange, respectively.

(C) The active site of CPAF. Omit electron density (2δ) for the residues around the active site of CPAF.

(D) Mutations of the catalytic triad abolish CPAF autocleavage and proteolytic cleavage of RFX5. (Top) For WT or various CPAF mutants, shown on the left and right are the samples before and after incubation (for 6 hr) at room temperature, respectively. (Bottom) Sample shown on the top panel was mixed with RFX5 and incubated at 4°C for 10 min. The residual RFX5 was visualized by Coomassie blue staining following SDS-PAGE.

(E) Superposition of CPAF with tricorn around the active site. Residues from CPAF and tricorn are shown in magenta and gray, respectively.

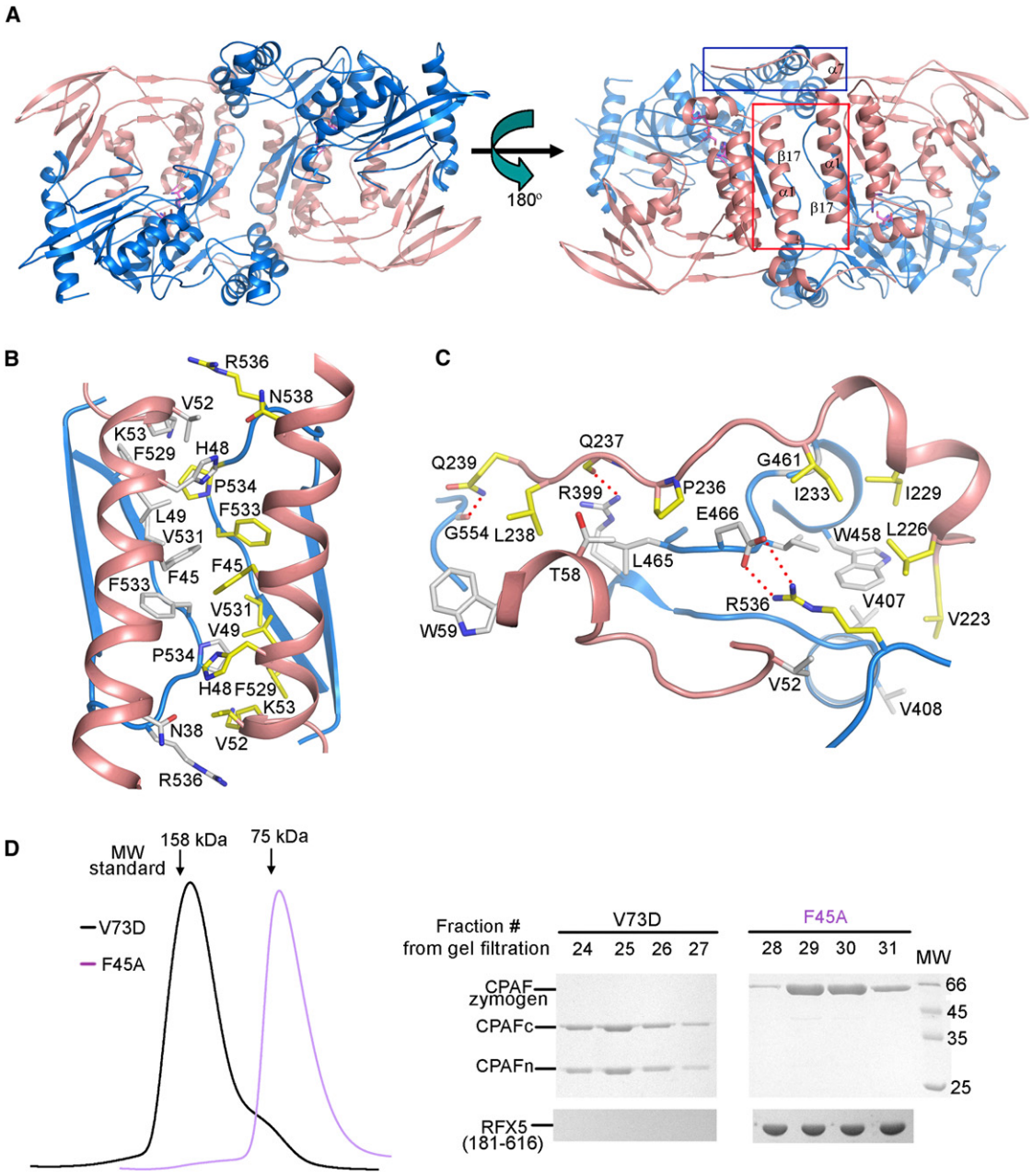

Figure 3. Homodimeric Assembly of CPAF

(A) CPAF forms a homodimer in the crystals. Two different views of the CPAF homodimer in the crystal structure. The two regions involved in CPAF homodimerization are highlighted in red and blue frames. The three catalytic residues are shown in stick representation.

(B and C) The detailed interactions around the two regions in (A) highlighted red and blue, respectively.

(D) The monomeric CPAF mutant fails to autocleave and process RFX5. Shown at the bottom right is the residual RFX5 after incubation with the corresponding protein shown on the top at 4°C for 10 min.

CPAF homodimerization, even transiently, may be required for its autocleavage. This conclusion is not necessarily inconsistent with our observation that formation of a stable CPAF homodimer is induced by its autocleavage (Figure 1D). This is because the wild-type monomeric zymogen may be able to form a transient homodimer, especially at a high concentration, allowing the dimerized CPAF zymogen to possess marginal activity and process each other. The initial processing, in return, further induces stable homodimerization that is required for the full activity of CPAF. It was suggested (Paschen et al., 2008) that CPAF activation may mimic that of initiator caspases in which proximity-dependent transient homodimerization followed by the formation of a stable homodimer (Boatright et al., 2003; Donepudi et al., 2003; Riedl and Salvesen, 2007; Yan et al., 2006) is required their full activity. Our data further strengthen this idea.

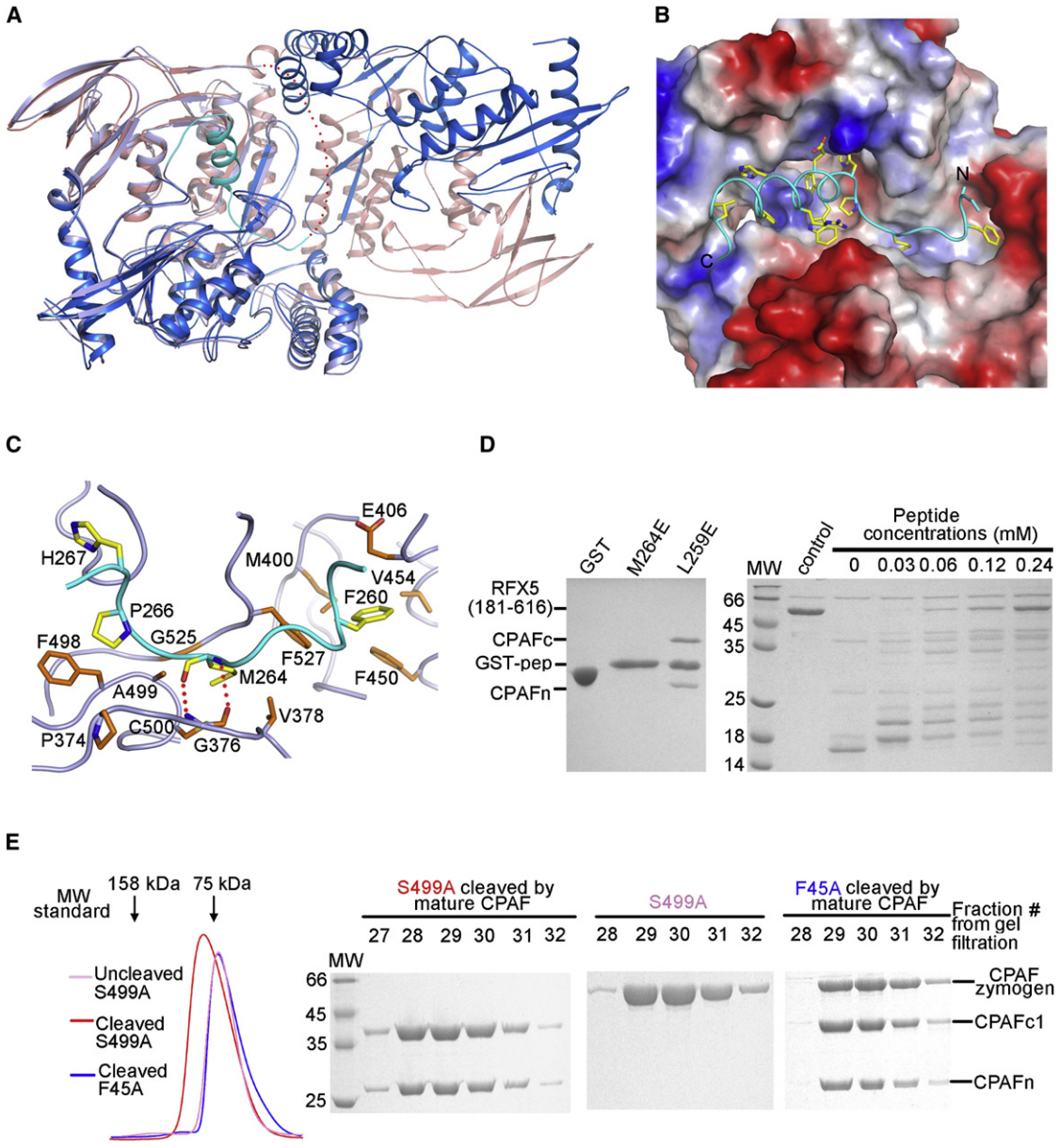

Figure 4. An Internal Inhibitory Segment Binds to the Active Site of CPAF and Blocks Its Homodimerization

(A) Superposition of one CPAF zymogen molecule (slate) with the homodimer of the mature CPAF. The well-ordered peptide (residues 258–283) from zymogen absent in the mature CPAF is shown in cyan, whereas the red dashed line (residues 223–257) represents the disordered peptide in CPAF zymogen.

(B) Overall view of the catalytic groove in CPAF zymogen (represented by its electrostatic surface) bound by the peptide.

(C) The detailed interactions between N terminus of the inhibitory peptide with CPAF active site.

(D) An isolated peptide derived from the inhibitory segment interacts with the mature CPAF and inhibits its proteolytic activity. GST-fused peptide (residues 258–283) with mutation as indicated was used to pull down the mature CPAF. (Left) After extensive washing, the bound proteins visualized by Coomassie blue staining following SDS-PAGE are shown. (Right) The activity of CPAF to degrade RFX5 is inhibited by the peptide L259E.

(E) First cleavage of CPAF promotes its homodimerization. Shown on the left panel is superposition of the gel filtration chromatograms for the CPAF mutant S499A cleaved by the mature CPAF, uncleaved S499A, and F45A cleaved by the mature CPAF. S499A and F45A were incubated with the mature form CPAF at room temperature for 6 hr before subjected to gel filtration assay.

Autoinhibition of CPAF Zymogen by an Internal Inhibitory Segment

To understand CPAF activation mechanism, we determined the crystal structure of a CPAF zymogen (S499A) (Table S1). The two CPAF zymogen molecules in each asymmetric unit do not form a homodimer as observed in the mature CPAF (data not shown), but the overall structure of a single CPAF zymogen is similar to that of its mature form (Figure 4A). The most striking difference between them is that the active site of CPAF zymogen is blocked by a peptide (residues 258–283) (Figure 4A), completely filling the

active site of CPAF (Figure 4B). Recognition of this peptide by the active site is dominated by two regions of contacts. One primarily involves hydrophobic contacts of the N-terminal rigid coil against the core domain of CPAF. At its center, Met264 nicely fits into the hydrophobic pocket formed by Val378, Cys500, Gly525, F527, and the Cα atom of Ala499. Additionally, a pair of main-chain hydrogen bonds is made between Met264 and Gly376 (Figure 4C). Van der Waals contacts of three bulky residues, Phe268, Trp269, and Tyr276, with their respective neighboring residues dominate interactions of the other binding region (data not shown).

The structure reveals that CPAF zymogen is inactive because the substrates are unable to gain access to the substrate-binding pocket (Figure 4B). To test whether the isolated peptide interacts with the mature CPAF, we made a peptide mutant L259E, as its wild-type was efficiently cleaved by the mature CPAF (Figure S4). The peptide mutant was significantly compromised in its cleavage by CPAF (Figure S4), but they still interacted with each other (Figure 4D, left panel). As expected, the proteolytic activity of CPAF to degrade RFX5 was substantially inhibited by the peptide mutant L259E (Figure 4D, right panel). Supporting the structural observation (Figure 4C), the peptide mutant M264E showed no detectable interaction with the mature CPAF (Figure 4D, left panel).

Residues 223–257 preceding the peptide bound to the active site have no clear electron density in CPAF zymogen, but structural comparison indicates that they wobble around one CPAF homodimer interface (Figure 4A). Thus, the covalent linkage in this interdomain region would conceivably impose a structural hindrance on CPAF homodimerization, which can be partially relieved through cleavage after Met242. In support of this hypothesis, the catalytic mutant S499A, following processing by the active CPAF, was induced to shift to a higher molecular weight (Figure 4E, left panel), indicating that cleavage of this site may further stabilize the transient homodimer of CPAF. By contrast, the monomeric mutant F45A was eluted only at the position of monomer even after cleavage by the active CPAF (Figure 4E, left panel). Interestingly, although both S499A (Figure 4E, second panel from left) and F45A (Figure 4E, right panel) can be cleaved by the mature CPAF to generate CPAFc1 and CPAFn, they failed to undergo further processing and achieve full activation. Taken together, these results demonstrate that the internal segment (residues 243–283, referred to as the inhibitory segment hereafter) blocks substrate binding and sequesters CPAF in a monomeric state.

Assembly of the Catalytic Triad Induced by an Activation Switch upon CPAF Homodimerization

In CPAF zymogen, S499A is located immediately underneath the carbonyl carbon atom of Met264 (Figure 4C), suggesting that the peptide bond between Met264 and Val265 can be nucleophilically attacked by Ser499. Indeed, an intermediate (Figure 1A, labeled as CPAFc2) was generated by cleavage after Met264. Thus, the catalytic nucleophile and its attacked atom are already properly positioned in the dormant CPAF. However, autoprocessing of the second cleavage site was always dependent on the first one after Met242 (Figures 1A and 3D), which can facilitate CPAF homodimerization (Figure 4E). Additionally, the cleaved monomeric mutant F45A was unable to undergo further processing (Figure 4E). These results strongly suggest that CPAF homodimerization triggers conformational changes required for its full catalytic activity.

Indeed, dramatic conformational changes occur to residues Val550–Glu559 (loop L1) (Figure 5A). Following homodimerization, the N terminus (residues 550–556) of this loop swings about 40 degrees toward α13, allowing Arg551 to salt bond with Asp510 and make van der Waals contact with Val506 (Figure 5A). By contrast, the C terminus of this loop (residues 557–559) is turned inward toward the active site of CPAF and packs against the loop L2 harboring Ala524 (Figure 5A). In particular, Glu558 moves about 8.0 Å toward His105 (Figure 5A), enabling them to form a water-mediated hydrogen bond. On the other hand, interaction of the C terminus of L1 with loop L2 in the mature CPAF causes flipping of Ala524 (Figure 5B), which likely, in turn, drives the side chain of His105 to rotate about 90 degrees. This not only shortens the distance between His105$N^{\varepsilon 2}$ and Ser499O^{γ}, but also allows His105$N^{\varepsilon 2}$ to be properly oriented (Figure 5B), making it possible for them to form a hydrogen bond. These structural analyses indicate that conformational changes in CPAF following homodimerization induce assembly of its water-mediated catalytic triad.

Then what is the driving force to trigger the conformational changes in L1 during CPAF homodimerization? In the mature CPAF, the C terminus (residues 223–239) of CPAFn from one molecule interacts with CPAFc from the other (Figure 3C). In contrast, this segment exhibits no clear electron density and is supposed to be disordered in CPAF zymogen. Structural comparison indicates that this peptide from one CPAF monomer would clash with L1 from the other one if the conformation of the latter remained unchanged during homodimerization (Figure 5C). Thus, this peptide likely acts as a trigger to initiate conformational changes in L1 that eventually lead to assembly of the water-mediated catalytic triad. (Therefore, we designate this peptide as an activation switch.) In support of this, a CPAF mutant with a deletion of six residues (234–239) from the activation switch that makes it too short to reach L1, was unable to autocleave even incubated at room temperature for 6 hr (Figure 5D). Similar results were also obtained for the mutations of Arg551 and Ile557 (Figure 5D). In complete agreement with the structural observation, the deletion mutant was significantly compromised in its further processing following cleavage by the mature CPAF (Figure 5D). But incubation of the cleaved deletion mutant at room temperature for a longer time (about 12 hr) generated a small fraction of the "mature form" of CPAF. Although this mature form of CPAF generated no effect on its homodimerization, it had a significantly diminished activity of degrading RFX5 (Figure 5E). As expected, the deletion mutant lacking the first autocleavage site resulted in its failure to be processed by the mature CPAF (Figure 5D).

Lactacystin Is a Covalently Bound Inhibitor of CPAF

CPAF was proposed (Zhong et al., 2001) to possess proteasome-like activity, because its activity could not be blocked by protease inhibitors other than the proteasome-specific inhibitor lactacystin (Zhong et al., 2001), an irreversible inhibitor that blocks proteasome activity through its hydrolyzed product, *clasto*-lactacystin β-lactone (omuralide) (Figure 6A) (Dick et al., 1997; Groll et al., 1997). Inhibition of CPAF by lactacystin was

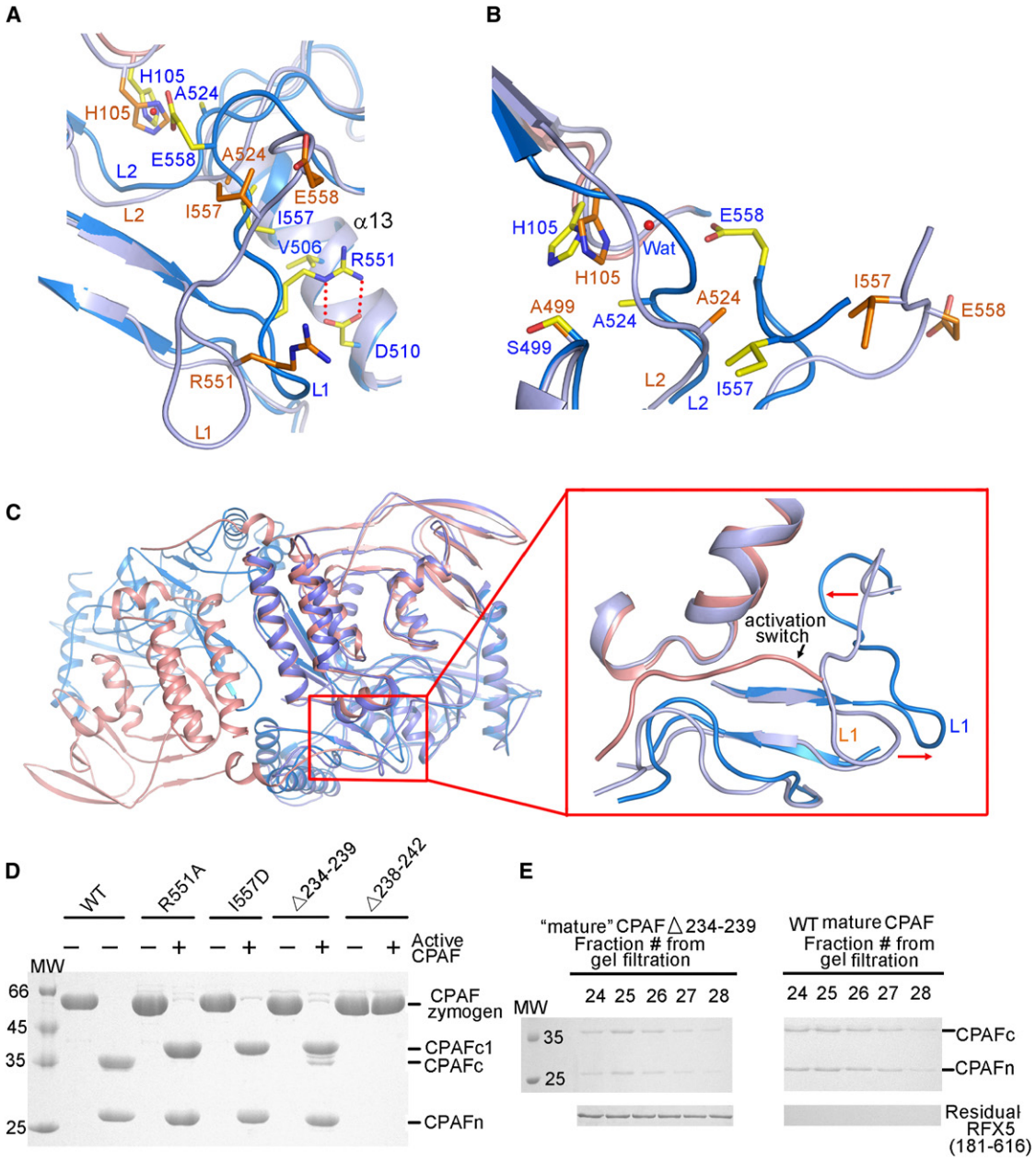

Figure 5. CPAF Homodimerization Triggers Assembly of the Water-Mediated Catalytic Triad

(A) Conformational changes occur to loop L1 (residues 550–559) upon CPAF homodimerization. Close-up view of structural comparison around loop L1 between CPAF zymogen (slate) and its mature form.

(B) Conformational changes in loop L2 (residues 522–527) are induced by those in loop L1. Close-up view of comparison around loop L2 (residues 522–527) between CPAF zymogen and its mature form.

(C) The activation switch, as labeled, would clash with L1 if the latter remained unchanged following CPAF homodimerization. (Left) The superimposition of a CPAF homodimer with one CPAF zymogen molecule. (Right) A close-up view of the region highlighted in the red frame on the left.

(D) A shortened activation switch or an unstabilized L1 significantly compromises CPAF autocleavage. For various CPAF mutants, the left lane represents the sample incubated at room temperature for 6 hr, and the right lane represents the sample cleaved by the active CPAF. For WT CPAF, the left and right lanes are the samples before and after incubation (for 6 hr) at room temperature, respectively. "Δ" represents the truncated mutant.

(E) CPAF with a shortened activation switch still forms a homodimer in solution but exhibits little proteolytic activity. For WT mature CPAF and the deletion mutant, protein from fraction 25 shown on the top panel was diluted 5-fold for the activity assay. The assay was performed as described in Figure 1B.

further verified by our current data (Figure 1C). To elucidate the inhibition mechanism, we determined the crystal structure of CPAF complexed with lactacystin (Table S1).

The homodimer observed in the free mature CPAF also exists in the structure of CPAF-lactacystin complex (Figure S5), indicating that inhibition of CPAF by lactacystin is not through

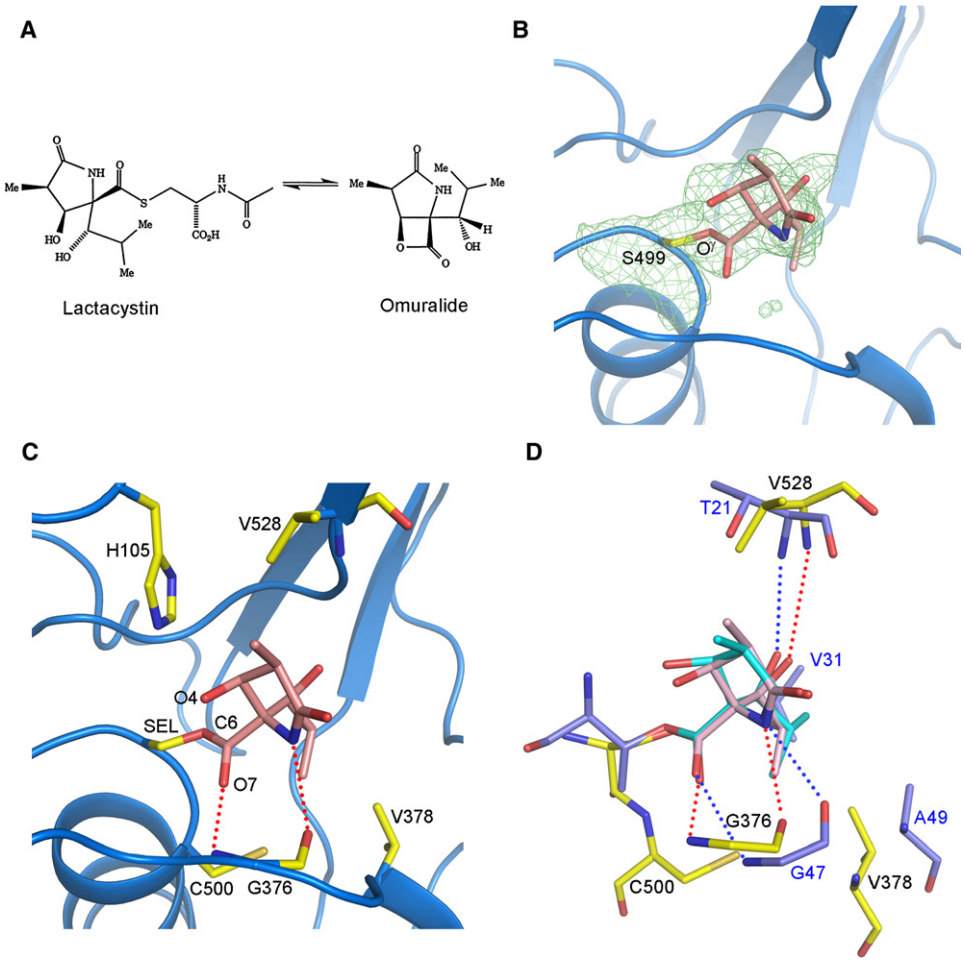

Figure 6. Lactacystin Covalently Binds to CPAF

(A) Equilibration of lactacystin with *clasto*-lactacystin β-lactone in solution (omuralide) (Dick et al., 1997).

(B) Omit electron density (2δ) around Ser499 in the structure of CPAF-omuralide complex. The model of omuralide (in pink) was built into the density. The side chain of Ser499 is shown in yellow.

(C) Specific recognition of omuralide by CPAF. The side chains of CPAF are colored in yellow and omuralide in pink. "SEL" represents the ester product formed between S499 and omuralide.

(D) Structural comparison between CPAF-omuralide (in pink) and proteasome-omuralide (in cyan) complexes. Residues from proteasome and CPAF are colored in slate and yellow, respectively. Hydrogen bonds in omuralide-CPAF and omuralide-proteasome complexes are shown in red and blue dashed lines, respectively.

disrupting CPAF homodimerization. A difference electron density map clearly shows that lactacystin binds around Ser499. The continuous electron density following Ser499O$^{\gamma}$ (Figure 6B) indicates that it has covalently linked to omuralide, which can cause irreversible inhibition of CPAF. Supporting this structural observation, CPAF activity was nearly killed at higher concentrations of lactacystin (Figure 1C). The covalently linked complex in the structure may result from the nucleophilic attack of Ser499O$^{\gamma}$ on the C6 in omuralide, which can be facilitated by the hydrogen bond formed between O7 of omuralide and the amide nitrogen of Gly376 (Figure 6C). This reaction can result in the formation of an ester bond in the active site of CPAF. A similar mechanism was proposed in the inhibition of proteasome by lactacystin (Groll et al., 1997, 2006a), which involves displacement of nucleophilic water molecules by the C4-hydroxy group generated through opening of the γ-lactam, thus blocking the attack of Thr1O$^{\gamma}$-CO ester bond (Groll et al., 2006b). In serine proteases, the nucleophilic water is assisted by the His residue from the catalytic triad for attacking the transition state intermediate acyl-enzyme (Hedstrom, 2002). Although the nucleophilic water molecule is disordered in the free active CPAF, it should exist in substrate-enzyme complex to form a hydrogen bond with H105 and make nucleophilic attack on the acyl-enzyme to complete the hydrolyzing reaction. In CPAF-lactacystin, the C4-hydroxy group is 3.6 Å from His105N$^{\varepsilon 2}$, suggesting that it may interfere with formation of the hydrogen bond between His105 and the nucleophilic water molecule. This would explain, at least in part, why the ester bond in CPAF-lactacystin complex is not hydrolyzed as in the case of proteasome-lactacystin complex (Groll et al., 2006a).

The specificity of omuralide for CPAF is determined by both hydrophobic contacts and hydrogen bonds (Figures 6C).

Structural comparison indicates that recognition of omuralide by CPAF and proteasome is through highly conserved interactions, particularly the hydrogen bonds (Figure 6D), indicating that CPAF may mimic host proteasome at least in lactacystin binding. By contrast, Ser protease inhibitors TPCK and PMSF are as unlikely to form hydrogen bonds with CPAF as those observed in CPAF-lactacystin complex, because no polar group exists in their benzene ring. This may provide an explanation of why CPAF activity is insensitive to them (Zhong et al., 2001). Our results not only reveal the inhibition mechanism of CPAF by lactacystin, but also provide structural evidence that lactacystin can inhibit proteases in addition to proteasome.

DISCUSSION

CPAF Defines a Unique Family of Ser Proteases

Structural comparison (Figures 2B and 2E) appears to support that CPAF is a CPP. However, it is important to note that CPAF is different than these proteases in that its catalytic residues are contributed by two distinct subunits. CPPs, in general, recognize a C-terminal tripeptide including the carboxy terminus in the substrates to cleave off the C-terminal residues from the substrates (Rawlings et al., 2008). Although the water-mediated catalytic triad of CPAF mimics the catalytic tetrad of the tricorn protease, other residues around the active site are not conserved. In particular, the two basic residues, Arg131 and Arg132, important for the tricorn protease to anchor the substrate C terminus (Brandstetter et al., 2002) are not conserved in the active site of CPAF. CT441 in *C. trachomatis* was recently shown to be a CPP (Lad et al., 2007). However, compared to CT441, CPAF has lower sequence homology to the known CPPs. The conclusion that CPAF does not belong to the CPP family is further supported by the following biochemical evidence. First, the C-terminal sequences of the substrates are not required for their proteolytic cleavage by CPAF. Among the known CPAF substrates, including RFX5, keratin 8, PUMA (Pirbhai et al., 2006), PARP, and Cyclin B1 (Paschen et al., 2008), no sequence homology exists at their C termini. Second, CPAF does not seem to process the C termini of its substrates. Both the N- (Figure S1) and C-terminal (Figure 1B) fragments of RFX5 were processed into multiple smaller fragments, suggesting that CPAF possesses an endopeptidase activity. This conclusion is consistent with the report that CPAF cleaved off both the N-terminal head and C-terminal tail domains from keratin 8 (Dong et al., 2004a). Third, all three autocleavage sites of CPAF are located in the middle of its sequence. Thus, CPAF does not recognize its own C-terminal sequence for autoprocessing. The C-terminal carboxylate of CPAF is more than 300 residues away from any of the three autocleavage sites and is, therefore, unlikely involved in the recognition of the inhibitory segment for cleavage. This is consistent with the fact that the C terminus (residues 258–283) of the inhibitory segment can be cleaved by the mature CPAF (Figure S4), although it shares no homology with the C-terminal sequence of CPAF full-length molecule (Figure S3). Finally, the mature CPAF can still bind to Ni resin via the His tag fused to the C terminus of CPAF, indicating that the CPAF C terminus was not cleaved during activation. It is clear that CPAF may appear to maintain a structure similar to that of CPPs but has evolved a distinct enzymatic activity.

Model on CPAF Activation

In this current study, we have provided evidence that the highly purified recombinant CPAF can undergo *trans*-autocatalytic cleavage (Figure 1A) and thereby promote homodimer formation (Figure 4E), leading to conformational changes and formation of the catalytic triad (Figure 5). This results in further processing of the internal inhibitory segment to completely free the catalytic site. The observations that a variant of the inhibitory peptide interacted with CPAF and inhibited its activity (Figure 4D) strongly support that activation of CPAF is regulated via a multistep cleavage of the inhibitory segment. This multistep model is consistent with previous in vivo data that an intermediate fragment recognizable by an anti-CPAFc antibody was repeatedly detected during chlamydial infection (Dong et al., 2004b; Heuer et al., 2003).

Step 1: Transient homodimerization triggers the first cleavage between Met242 and Arg243, promoting the formation of more stable homodimers of CPAF (Figure 7). Transient homodimerization can take place in vitro by increasing concentrations of CPAF zymogen (Figure 1A). In further support of this possibility, forced clustering of CPAF by fusing to a bacterial gyrase resulted in CPAF activation in human cells (Paschen et al., 2008). A transient CPAF homodimer may possess weak activity to initiate the proteolytic cleavage. In CPAF homodimer, there is a long distance between the initial cleavage site of one CPAF molecule and the active site of the other (Figure 3A). Therefore, we propose that cleavage of this occurs through intertransient homodimers of CPAF (in *trans*). Supporting the *trans* autocleavage are the observations that in vitro autoprocessing of CPAF is concentration dependent (Figure 1C, right panel) and the catalytic mutant S499A was processed by the mature CPAF (Figure 4E). We can further speculate that the driving force for CPAF activation derives from homodimerization preceding proteolytic processing. Supporting this hypothesis is the observation that the monomeric mutant F45A failed to undergo autoprocessing (Figure 3D). It is noteworthy to point out that, although CPAF activation in a cell-free system is initiated strictly via an autoprocessing mechanism, we still cannot rule out the possibility that other protease(s) or cofactor(s) are involved in CPAF activation in vivo during chlamydial infection.

Step 2: The initial proteolytic cleavage after Met242 not only promotes homodimerization of CPAF (Figure 4) but also frees the activation switch, both of which are required for assembly of the water-mediated catalytic triad (Figure 5).

Step 3: Assembly of the water-mediated catalytic triad enables CPAF to further cleave the inhibitory segment (Figure 7). The observation that the catalytic mutant S499A was not cleaved between Met264–Val265 by the active CPAF (Figure 4E) strongly suggests that cleavage of this site is in *cis*. Removal of residues 243–264 through cleavages of the above two sites cannot only further enhance homodimerization of CPAF but also substantially reduce the binding affinity of the inhibitory segment with the active site, promoting release of its remaining part (265–283) from the active site and subsequent cleavage after Ser283 (Figure 7). Thus, the three proteolytic cleavage steps, which each depend on their previous one, result in complete removal of the inhibitory segment and full activation of CPAF.

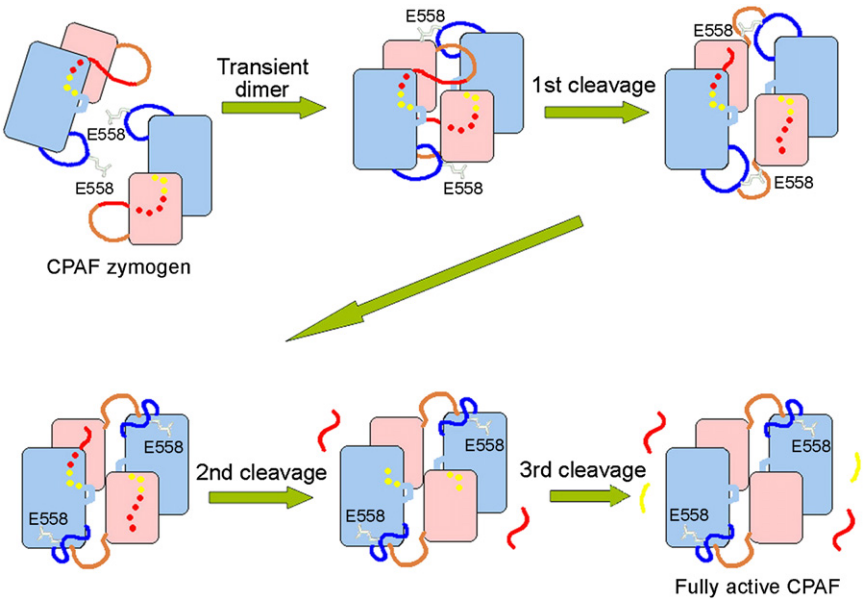

Figure 7. Schematic Diagram of CPAF Activation

The zymogen CPAF is kept dormant by the internal inhibitory segment (in red and yellow). Formation of a transient CPAF homodimer leads to autocleavage of the first cleavage site after Met242, promoting homodimerization of CPAF. The freed activation switch (in orange) in CPAFn (salmon) induces conformational change in loop L1 of CPAFc (blue) from the other CPAF monomer. Thus, Glu558 in L1 consequently moves close to His105 (data not shown), forming a water-mediated catalytic triad and leading to the cleavage after Met264. Removal of the peptide (residues 243–264, in red) diminishes binding affinity of the inhibitory segment with the active site of CPAF and promotes release of the remaining portion (residues 265–283, yellow dots) and cleavage after Ser283.

The structural data suggest that CPAF may mimic caspases for initiation of its activation, but different mechanisms follow to achieve their full activation; caspase homodimerization results in formation of the substrate-binding sites (Riedl and Salvesen, 2007), whereas CPAF's active site is preformed and homodimerization triggers realignment of its catalytic triad. Other Ser or Cys proteases involving homodimerization can result in formation of the composite substrate-binding groove (Lorenz et al., 2006) or a single active site at the homodimerization interface (Wlodawer and Gustchina, 2000). One exception to this is human cytomegalovirus (HCMV) protease in which homodimerization results in stabilization of the oxyanion hole (Batra et al., 2001). CPAF differs from these proteases in that its substrate-binding site in its zymogen is preformed and CPAF homodimerization triggers realignment of catalytic triad for its activation. Our results, therefore, reveal a distinct mechanism by which homodimerization regulates the catalytic activity of a Ser protease.

CPAF Activity Regulation in Chlamydial Biology and Pathogenesis

The complex regulation mechanism for controlling CPAF activity may have been evolved by Chlamydia as a result of the intricate chlamydial interactions with host cells. The concentration-dependent activation cascade of CPAF may provide Chlamydia additional means for regulating CPAF activity. CPAF does not accumulate inside chlamydial inclusion to any large amount, although it is synthesized by the organisms inside the inclusion. The yet to be secreted CPAF can remain dormant due to lack of critical concentration required for triggering CPAF activation, thus protecting Chlamydia's own proteins from the degradation by CPAF. This assumption gains supports from the finding that, although CPAF protein was detected inside inclusions as early as 12 hr postinfection, clear CPAF secretion and activity were only detected 24 hr after infection (Heuer et al., 2003; Shaw et al., 2002; Zhong et al., 2001). Chlamydia may have also taken advantage of the concentration-dependent activation of CPAF to avoid rapid destruction of host cells when Chlamydia still needs the integrity of host cells for completing its own replication. Supporting this hypothesis, the overall CPAF activity peaked 36–48 hr after infection, when the amount of CPAF had reached a plateau in the cytoplasm of the infected cells and most intracellular chlamydial organisms had already matured into the infectious elementary bodies and were ready to exit the infected cells (Heuer et al., 2003). The controlled CPAF activation is especially important during persistent infection, when chlamydial organisms hide inside host cells in a nonproductive and noninfectious form for long periods of time. Indeed, under persistent infection conditions, CPAF activity was maintained at a minimal level (Heuer et al., 2003; Shaw et al., 2002; Zhong et al., 2001).

Substrate Specificity

Although CPAF has been shown to be able to cleave multiple host proteins, its substrate specificity still remains unknown. The observations that the C terminus of the inhibitory segment binds to the active site of CPAF (Figure 4B) and itself can be cleaved by the active CPAF (Figure S4) indicate that CPAF zymogen essentially represents an enzyme-substrate complex, which may provide significant insights into the substrate specificity of CPAF.

Recognition of the peptide by the active site of CPAF is primarily through hydrophobic interactions (Figure 4B). Extensive interactions of Met264 with a hydrophobic pocked around the active site of CPAF (Figure 4C) indicate that CPAF has a preference for substrates with hydrophobic residues at P_1 position. But due to the limited size of this pocket, a bulky hydrophobic residue like Trp would be unfavorable for substrate binding. Interestingly, recognition of lactacystin is predominantly through the S_1 site (Figure 6C), suggesting that it may play an important role in determining the substrate specificity of CPAF. By contrast, residues at the positions of P_2, P_3, and P_4 make no contact with their neighboring residues. Phe260 at P_5 position makes extensive hydrophobic contacts with CPAF (Figure 4C), but mutation of this residue slightly affected cleavage of the GST-peptide by the mature CPAF (Figure S4). Interestingly, although the side

chain of Leu259 at P_6 makes no contact with other residues, mutation of this residue L259E significantly compromised its cleavage by the mature CPAF (Figure S4) when the peptide (residues 258–283) was used as the substrate.

The side chain of Val265 turns itself outward of the active site and is not involved in peptide recognition by the active site. Thus, the residue at the $P_{1'}$ position may not have much influence on substrate recognition, although the small ones might be preferred by CPAF. The $P_{2'}$ position is occupied by Pro266 that faces the bottom of the active site and makes hydrophobic contacts with Phe498 and Pro374 (Figure 4C), thus significantly circumscribing the size of a residue at this position. It is, therefore, conceivable that CPAF would prefer small hydrophobic residues at $P_{2'}$. Like Pro266, His267 at $P_{3'}$ faces the inside of the active site and is completely buried. But it is positioned in a large enough hydrophobic pocket to accommodate the bulky hydrophobic residues like Phe (Figure 4C). Thus, CPAF may recognize more varied residues at $P_{3'}$ than at $P_{2'}$. Phe268 (at $P_{4'}$) and Trp269 (at $P_{5'}$) interact extensively with the active site of CPAF. Thus, CPAF can prefer bulky residues at these two positions.

Although more studies, including kinetics and mutagenesis, are needed to further map the cleavage motifs of CPAF, the information derived from recognition of the inhibitory peptide and lactacystin by CPAF should be valuable in identifying additional substrates of CPAF and designing small molecular inhibitors as the therapeutic agents in a variety of clinical situations. Although CPAF has been demonstrated to be a virulence factor in chlamydial pathogenesis, no attenuated chlamydial strains have been generated due to the difficulty in genetic manipulation of Chlamydia. Using the knowledge gained from the current study to develop CPAF-specific inhibitors may represent a viable approach for attenuating chlamydial pathogenicity.

EXPERIMENTAL PROCEDURES

Protein Expression and Purification

All of the constructs were generated by the standard PCR-based cloning strategy, and their identities were confirmed by sequencing. All of the CPAFs (residues 25–609), wild-type or various mutants, were cloned into the vector pET30a (Novagen) unless specified otherwise. All of the proteins were expressed in *Escherichia Coli* strain BL21 (DE3). The proteins were first purified on Ni-resin and then further fractionated by anion ion exchange (Source-15Q, Pharmacia) and gel filtration chromatography (Superdex-200, Pharmacia). The mutant CPAF S499A protein thus purified was directly used for crystallization, whereas the wild-type CPAF was first left at room temperature for 6 hr to allow it to be fully autoprocessed and then subjected to gel filtration chromatography again. The purified autocleaved CPAF was further concentrated to ~10.0 mg/ml for crystallization.

Crystallization and Data Collection

Crystals of the active CPAF, its complex with lactacystin, and mutant S499A were generated by mixing the complex with an equal amount of well solution by the hanging-drop vapor-diffusion method. The native active CPAF protein was crystallized in buffer containing 1.4 M Li_2SO_4, 0.1 M HEPES (pH 7.0). The crystals belong to the $P2_12_12_1$ space group, with two CPAF molecules in each asymmetric unit and a unit cell a = 61.30 Å, b = 152.37 Å, c = 162.58 Å, and $\alpha = \beta = \gamma = 90.0^\circ$. The mutant S499A was crystallized under the conditions of 3.9 M $NaNO_3$, 0.5 M NaCl, 0.08 M KCl, and 0.1 M Bis-Tris propane (BTP) (pH 8.0). The crystals belong to R32 and have a unit cell a = b = 192.67 Å, c = 338.87 Å, and $\alpha = \beta = 90.0^\circ$, $\gamma = 120^\circ$, with two CPAF molecules in each asymmetric unit. Crystals of active Se-Met CPAF were generated under the same conditions as those of the native one but belong to the $P4_12_12$ space group, with two CPAF molecules in each asymmetric unit and a unit cell a = b = 124.87 Å, c = 241.51 Å, and $\alpha = \beta = \gamma = 90.0^\circ$. Lactacystin (2 mM) was mixed with an equal volume of CPAF and incubated at 4°C for 6 hr and then used for crystallization. The crystals of the lactacystin-CPAF complex were generated in buffer-containing 15.0% PEG 4000 (v/v), 0.6 M $MgCl_2$, 0.1 M Tris (pH 8.5). Crystals were equilibrated in a cryoprotectant buffer-containing reservoir buffer plus 15.0% glycerol (v/v). The native and MAD data sets were collected at the BSRF (Beijing, China) beamline 3W1A and processed using the software Denzo and Scalepack (Otwinowski and Minor, 1997).

Structure Determination and Refinement

SOLVE (Terwilliger, 2003) was used to locate the positions of selenium. The initial phases from SOLVE were further improved by solvent flattening using RESOLVE (Terwilliger, 2003). A model was built into the MAD electron density map using the program O (Jones et al., 1991). The initial model was first subjected to rigid body refinement and then annealing, position, and B factor refinement using CNS (Brünger et al., 1998) against the MAD data set. The crystal structures of active native CPAF, CPAF zymogen, and CPAF-lactacystin complex were determined by molecular replacement using the program MolRep. The final refined atomic model in the active native CPAF contains residues 31–239, 284–601, and 427 water molecules, whereas, in the CPAF mutant, S499A contains residues 31–222 and 258–604 with no water molecules added.

In Vitro Enzymatic Activity Assay

The assay was carried out at 4°C in buffer containing 25 mM Tris (pH 8.0), 150 mM NaCl, and 3 mM dithiothreitol (DTT). Two RFX5 fragments (residues 1–180 and 181–616) were used as the substrates of CPAF at a concentration of ~50.0 μM. The mature CPAF was purified to homogeneity and used in each reaction at 0.5 μM. Reaction samples were taken out at different time points and applied to SDS-PAGE followed by Coomassie blue staining. To generate the variant of the mature form CPAF with deletion of six residues (234–239), the active CPAF was first incubated with CPAF zymogen containing deletion of six residues (234–239) for 6 hr at room temperature. The CPAF zymogen thus treated was completely cleaved into CPAFc1 and CPAFn. The reaction mixture was further subjected to anion ion exchange chromatography (Q-Sepharose, Pharmacia). Fractions containing CPAFc1 and CPAFn were collected and left at room temperature for 12 hr to generate more mature form CPAF and then subjected to gel filtration chromatography. The mature CPAF thus generated was used for its activity assay.

For the inhibition of CPAF by lactacystin (Sigma), a progressively increasing amount of lactacystin (0.06, 0.12, 0.24, 0.48, 0.96, and 1.92 mM) was used. The peptide (residues 258–283 from CPAF), wild-type or various mutants, were cloned into vector pGEX-6P-1 (Pharmacia) and purified using glutathione sepharose 4B. After removal of glutathione S-transferase (GST) by PreScission protease, the peptide was subjected to gel filtration for further purification. An increasing amount of the peptide with the mutation M264E (0.03, 0.06, 0.12, and 0.24 mM) thus purified was used for inhibition assay. The mature CPAF was incubated with lactacystin (for 30 min) or peptide (for 5 min) before the substrate was introduced.

Gel Filtration Assay

CPAF zymogens, wild type or its various mutants (S499A, F45A, and V73D), were subjected to gel filtration analysis after being purified by anion ion exchange (Source-15Q, Pharmacia). The CPAF mutants S499A and F45A were cleaved by the active CPAF at room temperature for 6 hr. The cleaved mutants were subjected to anion ion exchange (Source-15Q, Pharmacia) and gel filtration chromatography (Superdex-200, Pharmacia) to remove the active CPAF. Individual protein purified to homogeneity was incubated in assay buffer 25 mM Tris (pH 8.0), 150 mM NaCl, and 3 mM DTT for 10 min at 4°C. The proteins purified from anion ion exchange were subjected to gel filtration analysis (Superdex 200, Amersham Biosciences). Samples taken from relevant fractions were applied to SDS-polyacrylamide gel electrophoresis (SDS-PAGE) and visualized by Coomassie blue staining.

Pull-Down Assay

GST-mediated pull-down assay was used to investigate the interaction between the peptide (residues 258–283) mutants with the mature CPAF.

Approximately 200 μg of the peptide, fused with GST, was bound to glutathione sepharose and incubated with mature CPAF at 4°C for 5 min. After extensive washing using buffer containing 25 mM Tris (pH 8.0), 150 mM NaCl, and 3.0 mM DTT, the bound proteins were visualized by Coomassie staining following SDS-PAGE.

ACCESSION NUMBERS

The atomic coordinates of mature CPAF, mature Se-CPAF, CPAF zymogen (S499A), and CPAF-lactacystin complex have been deposited in the Protein Data Bank with accession numbers 3DOR, 3DJA, 3DPN, and 3DPM, respectively.

SUPPLEMENTAL DATA

The Supplemental Data include one table and five figures and can be found with this article online at http://www.cell.com/cell-host-microbe/supplemental/S1931-3128(08)00332-6.

ACKNOWLEDGMENTS

We thank Yuhui Dong and Peng Liu at the BSRF (Beijing, China) for assistance with the data collection and Dr. M. Groll for kindly providing the coordinates of proteasome-omuralide complex. This research is funded by the Chinese Ministry of Science and Technology.

Received: August 5, 2008
Revised: October 5, 2008
Accepted: October 17, 2008
Published: December 10, 2008

REFERENCES

Batra, R., Khayat, R., and Tong, L. (2001). Molecular mechanisms for dimerization to regulate the catalytic activity of human cytomegalovirus protease. Nat. Struct. Biol. *8*, 810–817.

Belland, R.J., Ouellette, S.P., Gieffers, J., and Byrne, G.I. (2004). Chlamydia pneumoniae and atherosclerosis. Cell. Microbiol. *6*, 117–127.

Boatright, K.M., Renatus, M., Scott, F.L., Sperandio, S., Shin, H., Pedersen, I.M., Ricci, J.E., Edris, W.A., Sutherlin, D.P., Green, D.R., et al. (2003). A unified model for apical caspase activation. Mol. Cell *11*, 529–541.

Brandstetter, H., Kim, J.S., Groll, M., and Huber, R. (2001). Crystal structure of the tricorn protease reveals a protein disassembly line. Nature *414*, 466–470.

Brandstetter, H., Kim, J.S., Groll, M., Gottig, P., and Huber, R. (2002). Structural basis for the processive protein degradation by tricorn protease. Biol. Chem. *383*, 1157–1165.

Brünger, A.T., Adams, P.D., Clore, G.M., DeLano, W.L., Gros, P., Grosse-Kunstleve, R.W., Jiang, J.S., Kuszewski, J., Nilges, M., Pannu, N.S., et al. (1998). Crystallography & NMR system: A new software suite for macromolecular structure determination. Acta Crystallogr D Biol. Crystallogr. *54*, 905–921.

Brunham, R.C., and Rey-Ladino, J. (2005). Immunology of Chlamydia infection: implications for a Chlamydia trachomatis vaccine. Nat. Rev. Immunol. *5*, 149–161.

Byrne, G.I., and Ojcius, D.M. (2004). Chlamydia and apoptosis: life and death decisions of an intracellular pathogen. Nat. Rev. Microbiol. *2*, 802–808.

Campbell, L.A., and Kuo, C.C. (2004). Chlamydia pneumoniae–an infectious risk factor for atherosclerosis? Nat. Rev. Microbiol. *2*, 23–32.

Danesh, J., Collins, R., and Peto, R. (1997). Chronic infections and coronary heart disease: is there a link? Lancet *350*, 430–436.

Dean, D., and Powers, V.C. (2001). Persistent Chlamydia trachomatis infections resist apoptotic stimuli. Infect. Immun. *69*, 2442–2447.

Dick, L.R., Cruikshank, A.A., Destree, A.T., Grenier, L., McCormack, T.A., Melandri, F.D., Nunes, S.L., Palombella, V.J., Parent, L.A., Plamondon, L., et al. (1997). Mechanistic studies on the inactivation of the proteasome by lactacystin in cultured cells. J. Biol. Chem. *272*, 182–188.

Donepudi, M., Mac Sweeney, A., Briand, C., and Grütter, M.G. (2003). Insights into the regulatory mechanism for caspase-8 activation. Mol. Cell *11*, 543–549.

Dong, F., Su, H., Huang, Y., Zhong, Y., and Zhong, G. (2004a). Cleavage of host keratin 8 by a Chlamydia-secreted protease. Infect. Immun. *72*, 3863–3868.

Dong, F., Pirbhai, M., Zhong, Y., and Zhong, G. (2004b). Cleavage-dependent activation of a chlamydia-secreted protease. Mol. Microbiol. *52*, 1487–1494.

Dong, F., Sharma, J., Xiao, Y., Zhong, Y., and Zhong, G. (2004c). Intramolecular dimerization is required for the chlamydia-secreted protease CPAF to degrade host transcriptional factors. Infect. Immun. *72*, 3869–3875.

Dong, F., Zhong, Y., Arulanandam, B., and Zhong, G. (2005). Production of a proteolytically active protein, chlamydial protease/proteasome-like activity factor, by five different Chlamydia species. Infect. Immun. *73*, 1868–1872.

Fan, T., Lu, H., Hu, H., Shi, L., McClarty, G.A., Nance, D.M., Greenberg, A.H., and Zhong, G. (1998). Inhibition of apoptosis in chlamydia-infected cells: blockade of mitochondrial cytochrome c release and caspase activation. J. Exp. Med. *187*, 487–496.

Fenteany, G., Standaert, R.F., Lane, W.S., Choi, S., Corey, E.J., and Schreiber, S.L. (1995). Inhibition of proteasome activities and subunit-specific amino-terminal threonine modification by lactacystin. Science *268*, 726–731.

Fischer, S.F., Vier, J., Kirschnek, S., Klos, A., Hess, S., Ying, S., and Häcker, G. (2004). Chlamydia inhibit host cell apoptosis by degradation of proapoptotic BH3-only proteins. J. Exp. Med. *200*, 905–916.

Greene, W., Xiao, Y., Huang, Y., McClarty, G., and Zhong, G. (2004). Chlamydia-infected cells continue to undergo mitosis and resist induction of apoptosis. Infect. Immun. *72*, 451–460.

Groll, M., Ditzel, L., Löwe, J., Stock, D., Bochtler, M., Bartunik, H.D., and Huber, R. (1997). Structure of 20S proteasome from yeast at 2.4 A resolution. Nature *386*, 463–471.

Groll, M., Huber, R., and Potts, B.C. (2006a). Crystal structures of Salinosporamide A (NPI-0052) and B (NPI-0047) in complex with the 20S proteasome reveal important consequences of beta-lactone ring opening and a mechanism for irreversible binding. J. Am. Chem. Soc. *128*, 5136–5141.

Groll, M., Larionov, O.V., Huber, R., and de Meijere, A. (2006b). Inhibitor-binding mode of homobelactosin C to proteasomes: new insights into class I MHC ligand generation. Proc. Natl. Acad. Sci. USA *103*, 4576–4579.

Hedstrom, L. (2002). Serine protease mechanism and specificity. Chem. Rev. *102*, 4501–4524.

Heuer, D., Brinkmann, V., Meyer, T.F., and Szczepek, A.J. (2003). Expression and translocation of chlamydial protease during acute and persistent infection of the epithelial HEp-2 cells with Chlamydophila (Chlamydia) pneumoniae. Cell. Microbiol. *5*, 315–322.

Jones, T.A., Zou, J.-Y., Cowan, S.W., and Kjeldgaard, M. (1991). Improved methods for building protein models in electron density maps and the location of errors in these models. Acta Crystallogr. A *47*, 110–119.

Lad, S.P., Yang, G., Scott, D.A., Wang, G., Nair, P., Mathison, J., Reddy, V.S., and Li, E. (2007). Chlamydial CT441 is a PDZ domain-containing tail-specific protease that interferes with the NF-kappaB pathway of immune response. J. Bacteriol. *189*, 6619–6625.

Liao, D.I., Qian, J., Chisholm, D.A., Jordan, D.B., and Diner, B.A. (2000). Crystal structures of the photosystem II D1 C-terminal processing protease. Nat. Struct. Biol. *7*, 749–753.

Lorenz, I.C., Marcotrigiano, J., Dentzer, T.G., and Rice, C.M. (2006). Structure of the catalytic domain of the hepatitis C virus NS2-3 protease. Nature *442*, 831–835.

Miyairi, I., and Byrne, G.I. (2006). Chlamydia and programmed cell death. Curr. Opin. Microbiol. *9*, 102–108.

Morrison, R.P., Belland, R.J., Lyng, K., and Caldwell, H.D. (1989). Chlamydial disease pathogenesis. The 57-kD chlamydial hypersensitivity antigen is a stress response protein. J. Exp. Med. *170*, 1271–1283.

Otwinowski, Z., and Minor, W. (1997). Processing of X-ray diffraction data collected in oscillation mode. In Methods in Enzymology, *Volume 76*, C.W. Carter, Jr., and R.M. Sweet, eds. (San Diego, CA: Academic Press), pp. 307–326.

Paschen, S.A., Christian, J.G., Vier, J., Schmidt, F., Walch, A., Ojcius, D.M., and Häcker, G. (2008). Cytopathicity of Chlamydia is largely reproduced by expression of a single chlamydial protease. J. Cell Biol. *182*, 117–127.

Perfettini, J.L., Darville, T., Dautry-Varsat, A., Rank, R.G., and Ojcius, D.M. (2002). Inhibition of apoptosis by gamma interferon in cells and mice infected with *Chlamydia muridarum* (the mouse pneumonitis strain of *Chlamydia trachomatis*). Infect. Immun. *70*, 2559–2565.

Pirbhai, M., Dong, F., Zhong, Y., Pan, K.Z., and Zhong, G. (2006). The secreted protease factor CPAF is responsible for degrading pro-apoptotic BH3-only proteins in Chlamydia trachomatis-infected cells. J. Biol. Chem. *281*, 31495–31501.

Rasmussen, S.J., Eckmann, L., Quayle, A.J., Shen, L., Zhang, Y.X., Anderson, D.J., Fierer, J., Stephens, R.S., and Kagnoff, M.F. (1997). Secretion of proinflammatory cytokines by epithelial cells in response to Chlamydia infection suggests a central role for epithelial cells in chlamydial pathogenesis. J. Clin. Invest. *99*, 77–87.

Rawlings, N.D., Morton, F.R., Kok, C.Y., Kong, J., and Barrett, A.J. (2008). MEROPS: the peptidase database. Nucleic Acids Res. *36*, D320–D325.

Riedl, S.J., and Salvesen, G.S. (2007). The apoptosome: signalling platform of cell death. Nat. Rev. Mol. Cell Biol. *8*, 405–413.

Shaw, A.C., Vandahl, B.B., Larsen, M.R., Roepstorff, P., Gevaert, K., Vandekerckhove, J., Christiansen, G., and Birkelund, S. (2002). Characterization of a secreted Chlamydia protease. Cell. Microbiol. *4*, 411–424.

Stephens, R.S. (2003). The cellular paradigm of chlamydial pathogenesis. Trends Microbiol. *11*, 44–51.

Stephens, R.S., Kalman, S., Lammel, C., Fan, J., Marathe, R., Aravind, L., Mitchell, W., Olinger, L., Tatusov, R.L., Zhao, Q., et al. (1998). Genome sequence of an obligate intracellular pathogen of humans: *Chlamydia trachomatis*. Science *282*, 754–759.

Tamura, T., Tamura, N., Cejka, Z., Hegerl, R., Lottspeich, F., and Baumeister, W. (1996). Tricorn protease–the core of a modular proteolytic system. Science *274*, 1385–1389.

Terwilliger, T.C. (2003). SOLVE and RESOLVE: automated structure solution and density modification. Methods Enzymol. *374*, 22–37.

Wlodawer, A., and Gustchina, A. (2000). Structural and biochemical studies of retroviral proteases. Biochim. Biophys. Acta *1477*, 16–34.

Yan, N., Huh, J.R., Schirf, V., Demeler, B., Hay, B.A., and Shi, Y. (2006). Structure and activation mechanism of the Drosophila initiator caspase Dronc. J. Biol. Chem. *281*, 8667–8674.

Zhong, G., Fan, T., and Liu, L. (1999). Chlamydia inhibits interferon gamma-inducible major histocompatibility complex class II expression by degradation of upstream stimulatory factor 1. J. Exp. Med. *189*, 1931–1938.

Zhong, G., Liu, L., Fan, T., Fan, P., and Ji, H. (2000). Degradation of transcription factor RFX5 during the inhibition of both constitutive and interferon gamma-inducible major histocompatibility complex class I expression in chlamydia-infected cells. J. Exp. Med. *191*, 1525–1534.

Zhong, G., Fan, P., Ji, H., Dong, F., and Huang, Y. (2001). Identification of a chlamydial protease-like activity factor responsible for the degradation of host transcription factors. J. Exp. Med. *193*, 935–942.